JOURNAL OF AIRCRAFT
Vol. 48, No. 1, January–February 2011

Flight Tests, Performances, and Flight Certification of a Twin-Engine Light Aircraft

Fabrizio Nicolosi,* Agostino De Marco,† and Pierluigi Della Vecchia‡
University of Naples "Federico II," 80125 Naples, Italy

DOI: 10.2514/1.C031056

This paper deals with flight-test activities performed on the P2006T, a twin-engine light aircraft recently designed and produced by Tecnam. Research activities and flight tests have been conducted during the flight certification of the P2006T for the normal category under European regulation CS-23. All the acquired data and flight results presented have been focused on both aircraft certification and aircraft performance, stability, and flight quality measurements. The data have been acquired through light, accurate, and reliable flight instrumentation available at the University of Naples "Federico II" department of aerospace engineering. Some flight data about aircraft leveled speed, stall speed, climb characteristics, and ground performances (takeoff and landing) will be presented. After preliminary flight tests, winglets have been designed and added to the final configuration in order to obtain good climb performances in one-engine inoperative conditions. Accurate stall tests have been performed in all configurations, and the influence of both the entry rate and the load factor on stall speed have been highlighted. Excellent ground performances have been measured with short takeoff and landing distances compared with similar airplanes. All measured flight performances can be considered very good for this aircraft category and have been used to demonstrate aircraft safety and to obtain CS-23 certification.

Nomenclature

AR	=	wing aspect ratio
a_Z	=	vertical acceleration, g
c	=	chord (also mean aerodynamic chord)
$C_{L\max}$	=	maximum lift coefficient, (nW/qS)
C_{Ls}	=	stall lift coefficient, (W/qS)
e	=	induced drag efficiency factor
Hp	=	pressure altitude, ft
n	=	load factor, a_Z/g
PIW	=	generalized power parameter
q	=	flight dynamic pressure, $\frac{1}{2}\rho V^2$
S	=	wing area
T	=	temperature
THP_r	=	thrust horse power required
V	=	flight speed
VIW	=	generalized velocity parameter
V_2	=	flight speed over obstacle (takeoff)
V_{CAS}	=	calibrated air speed (usually in kt)
V_{IAS}	=	indicated air speed (usually in kt)
V_{LOFF}	=	liftoff speed (takeoff)
V_{NE}	=	never exceed speed
V_R	=	rotation speed (during takeoff)
V_{REF}	=	reference flight speed over obstacle during approach (landing)
V_S	=	stall speed
V_{TD}	=	touchdown speed (landing tests)
W	=	generic aircraft weight during tests
W_{std}	=	standard aircraft weight
W_{TO}	=	maximum takeoff weight
X_{cg}	=	dimensional position of aircraft c.g. on mean aerodynamic chord
α	=	angle of attack, deg
β	=	angle of sideslip, deg
δ_a	=	aileron deflection, deg
δ_r	=	rudder deflection, deg
δ_S	=	stabilator deflection, deg
η_p	=	propeller efficiency
ρ	=	air density
ρ_0	=	sea level air density, standard atmosphere
Φ	=	bank angle, deg

Presented as Paper 2010-7513 at the AIAA Guidance, Navigation, and Control Conference Atmospheric Flight Mechanics 2010 Conference, Toronto, ON, Canada, 2–5 August 2010; received 7 April 2010; revision received 24 August 2010; accepted for publication 24 August 2010. Copyright © 2010 by the American Institute of Aeronautics and Astronautics, Inc. All rights reserved. Copies of this paper may be made for personal or internal use, on condition that the copier pay the $10.00 per-copy fee to the Copyright Clearance Center, Inc., 222 Rosewood Drive, Danvers, MA 01923; include the code 0021-8669/11 and $10.00 in correspondence with the CCC.

*Assistant Professor, Department of Aerospace Engineering (DIAS), Via Claudio 21; fabrnico@unina.it. Senior Member AIAA.

†Assistant Professor, Department of Aerospace Engineering (DIAS), Via Claudio 21; agodemar@unina.it. Senior Member AIAA.

‡Ph.D. Student, Department of Aerospace Engineering (DIAS), Via Claudio 21.

I. Introduction

THIS paper deals with flight-testing research activity performed on the P2006T aircraft, an innovative twin-engine airplane produced by Tecnam Aeronautical Industries (www.tecnam.com). A large amount of postdesign work and many flight tests have been carried out by the authors during the flight certification of this airplane according to the European Aviation Safety Agency (EASA) regulation CS-23 [1]. The design of this very light twin-engine propeller aircraft with a maximum takeoff weight (MTOW) of 1180 kg has been presented extensively by Nicolosi and Pascale in previous papers [2,3], and its main features are summarized in the next section.

The authors are involved in the flight-research activities of the Aircraft Design and Aeroflightdynamics Group at the University of Naples "Federico II," Department of Aerospace Engineering (DIAS). Researchers of this group have been gaining experience in flight testing since 1997. Light and ultralight airplanes have been one of author's focus in recent years. The details of past experiences are found in the cited [4–6]. Most of the flight-test work has dealt with aircraft flight certification and flight-quality assessment.

All flight data have been acquired through light, fast, and reliable flight instrumentation available at the DIAS. The importance of the reliability and accuracy of flight-test instrumentation has already been experienced by de Oliveira et al. [7], Coiro et al. [8], and Giordano et al. [9], and the instrumentation (both the sensors and the acquisition system) used is the evolution of that used for ultralight aircraft (ULM) flight tests since 1998. A continuous improvement of the sensors and the acquisition system has been realized during the past years. The present system represents a very good compromise

Table 1 P2006T aircraft geometric characteristics

Parameter	Value	Parameter	Value
Wing span	37.40 ft (11.4 m)	Fuselage length	28.50 ft (8.7 m)
Wing area, S	159.31 ft^2 (14.8 m^2)	Cabin width	48.03 in (1.22 m)
MAC, c	4.40 ft (1.34 m)	Cabin length (with baggage)	11 ft (3.35 m)
Wing aspect ratio, AR	8.76 (8.76)	Fuselage height	9.35 ft (2.85 m)

between cost and performance. Control surface deflections have been acquired through potentiometers, a very accurate inertial measurement unit (XBow AHRS400) has been used to measure angles, accelerations, and angular rates, and air data (flight speed and altitude) have been measured through accurate pressure transducers. The angle of attack and angle of sideslip have been measured through a mini-air data boom placed in the nose of the airplane. A fast and accurate acquisition system composed by a small Pentium PC with a 16 bit 32-channel A/D internal board has been used. The system is capable of very accurate data acquisition and storage with high frequency (up to 50 Hz). Almost all flight tests have been performed with a 10 Hz sampling rate. The system is also equipped with a dual-frequency Global Positioning System (GPS) for position and groundspeed (GS) measurements. The GPS is acquired simultaneously with other flight data and with a sample rate of 10 Hz.

The flight-test campaign for the P2006T aircraft has been particularly demanding in terms of the amount of analysis work and precision, due to certification requirements. Preliminary flight-performance measurements on a prototype have been very important in the first phase for the assessment of the aircraft design. Improvement of the aircraft design has been accomplished through flight tests. For example, early flights have been performed on the first prototype without a winglet. After preliminary flight measurements, the one-engine inoperative (OEI) rate of climb (RC) at MTOW has been acceptable for certification but inappropriate for the commercial success of the aircraft. The wingtip has been changed and an optimized winglet shape has been designed [2,3] at the DIAS, and flight tests have been performed with the winglet installed. The aerodynamic data collected during wind-tunnel tests performed at the DIAS on the P2006T aircraft model [2,3] have also been very important to predict flight data before measurement and to complete aircraft certification (i.e., wing aerodynamic loads).

Some flight data about aircraft leveled speed, stall speed, climb characteristics [in both all-engines operative (AEO) and OEI conditions], and ground performances (takeoff and landing) will be presented. Accurate stall tests have been performed in all configurations and the influences of both the entry rate (ER) and the load factor on stall speed have been highlighted. Excellent ground performances have been measured, with short takeoff and landing distances compared with similar airplanes. All measured flight performances can be considered very good for this aircraft category and have been used to demonstrate aircraft safety and to obtain CS-23 certification [1]. The process of flight-test data analysis and correction for flight performance estimation has been accurately done in accordance with the reference manual by Perkins et al. [10] and the books by Ward and Strganac [11] and by Kimberlin [12] that represent fundamental guides on this field. The importance of good flight-test planning and the focus on certification aspects is also highlighted in [13], although they are referred to in the sport-plane aircraft category.

As reported by Rogers [14], flight-test performance measurements are also fundamental as a base for flight-test teaching activities.

II. P2006T Aircraft

The Tecnam P2006T is a twin-engine four-seat general aviation airplane with fully retractable landing gear. The high-wing configuration provides stability, high visibility, and easy access to passengers and baggage.

The designer of the P2006T is Luigi Pascale, a former professor at the University of Naples, who had developed the project of this twin-propeller airplane at Tecnam Aircraft Industries since 2006. The basic idea of this design consists of having a four-seat aircraft with two light engines, usually employed in ULM. Thanks to this idea, with the P2006T, it is the first time that a twin-engine four-seat aircraft has entered into the same market (also with similar price) as single-engine four-seat aircraft, having similar weight and power specifications. The selected engine is the Rotax 912S, which is approved for automotive fuel, and it is Federal Aviation Regulation (FAR) 33 certified [15]. This engine is a recent design that has taken advantage of all the latest technologies developed for the automotive market. With respect to the standard general aviation engines, the Rotax 912S has a reduced frontal area, a better weight-to-power ratio, lower specific fuel consumption, lower propeller revolutions per minute (RPM) (i.e., higher efficiency and lower acoustic emissions), and more stable engine head temperatures (due to liquid cooling).

From Tables 1–5, we have reported all the main geometric characteristics, weights, c.g. ranges, propulsion data, and performances of the certified airplane (as measured at the end of the flight-test campaign). The three-view drawing of the P2006T aircraft is shown in Fig. 1, and a picture of the airplane during flight tests is presented in Fig. 2. In Fig. 3, we compare the weight characteristics of some four-seat aircraft (most of which have engine power in the range of

Table 2 P2006T aircraft weights and loading

Parameter	Value
MTOW, W_{TO}	2601 lb (1180 kg)
Maximum ramp weight	2601 lb (1180 kg)
Standard equipped weight	1675 lb (760 kg)
Standard useful load	926 lb (420 kg)
Limit load factors, n	$+3.8$ g/ -1.9 g

Table 3 P2006T aircraft propulsion characteristics

Parameter	Value
Engine model	Rotax 912S
Takeoff power	100 hp (73 kW)
Maximum continuous power	92.4 hp (69 kW)
Propeller (two blades, constant speed, full feathering)	MTV-21-A-C-F/CF178-05

Table 4 P2006T Performances as measured from flight-certification tests

Parameter	Value
Max speed at S/L (full throttle, max RPM)	154 kt
Cruise speed (75%, 7000 ft)	145 kt
Cruise speed (65%, 9000 ft)	135 kt
Stall speed flap down	47 kt
V_A (maneuvering speed)	116 kt
V_{NE} (never exceed speed)	168 kt
Max RC, S/L	1210 ft/ min
Max RC, S/L ,OEI	350 ft/ min
Service ceiling (twin engine)	12,800 ft
Single-engine ceiling	6600 ft
Takeoff distance	1260 ft (384 m)
Takeoff ground run	968 ft (295 m)
Landing distance	1263 ft (385 m)
Landing ground run	734 ft (224 m)

Table 5 Selected c.g. range for flight tests (useful load 420 kg)

	Max forward	Max aft
X_{cg}/c	16.5%	31%
Load	Pilot (90 kg)	Pilot (90 kg)
Condition	3 crew (270 kg)	2 crew, rear (160 kg)
	No baggage	80 kg baggage
	6- kg fuel	90 kg fuel

200–400). It is evident that, for the first time, it is possible to compare a twin-engine four-seat aircraft with a single-engine four-seat aircraft due to their similar weight and power specifications. Figure 4a shows the aircraft cockpit (with an electronic flight instrument system and digital instruments), and Fig. 4b shows the baggage compartment. The wide space available in the baggage compartment has been extremely useful to easily install all flight instrumentation and the acquisition system described in the next paragraph.

III. Flight-Test Instrumentation

Flight data have been acquired through light, fast, and reliable flight instrumentation. The choice of a particular flight-test instrumentation depends on the type of required flight-test campaign and on the desired accuracy. The importance of selecting reliable and accurate test instruments has emerged in a number of past experiences on similar airplanes [6–9,16]. The instrumentation used for the present research (both the sensors and acquisition system) is the evolution of that used for all ULM flight tests since 1998 [16]. The present system represents a very good compromise between cost and performance. The importance of accurate but affordable flight-test equipment in flight-test activity performed on light aircraft is also highlighted in [17]. The importance of research and teaching activities addressing the setup of a complete flight-test instrumentation system is emphasized in [18].

The flight data acquisition system consists of a central unit named CSYS (central system); see Fig. 5. It includes a small and light airborne computer equipped with dedicated cards for the conditioning and control of signals. All signals come from a set of flight sensors appropriately connected to a central unit.

The CSYS is a transportable and complete data acquisition system designed for the gathering of flight data, data storage on magnetic support, and date remote transmission in real time. It integrates a differential GPS and is easily interfaced with an AHRS-400 inertial measurement unit (see also Fig. 5) that is placed close to the aircraft c.g.. When equipped with an external radio modem, the system is able to transmit the data in real time to a remote ground station. During these flight certification tests, all data have only been recorded onboard on the magnetic support with a sample rate of 10 Hz.

The CSYS includes a National Instruments card, which is the main building block of the data acquisition hardware. Multiplexing, conditioning, and signal control technologies are embedded into the CSYS case. The system is able to acquire 32 analogue channels and six digital channels. It has four analog output ports, four USB ports, and other typical PC connections.

The aircraft is equipped with sensors for the acquisition and measurement of flight data. Pressure transducers have been installed to measure the speed and altitude. For these sensors, we have assessed an accuracy of about 0.5 kt on flight speed and 3 ft on altitude. A special sensor (mini-air data boom produced by SpaceAge Control, Inc.) for the measurement of the angle of attack and the angle of sideslip has been mounted on the nose of the aircraft (see

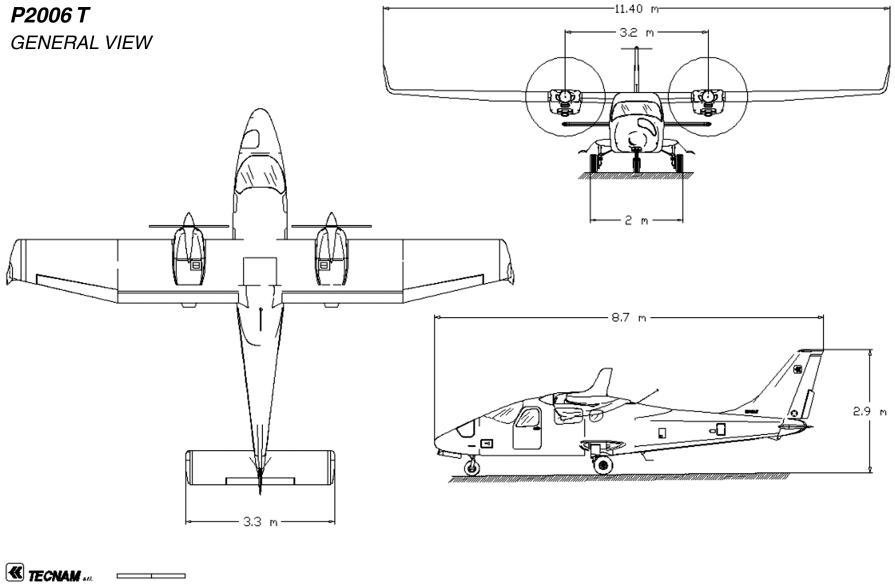

Fig. 1 Three-view drawing of P2006T aircraft. (Courtesy of Tecnam.)

Fig. 2 P2006T during flight tests. (Courtesy of Tecnam.)

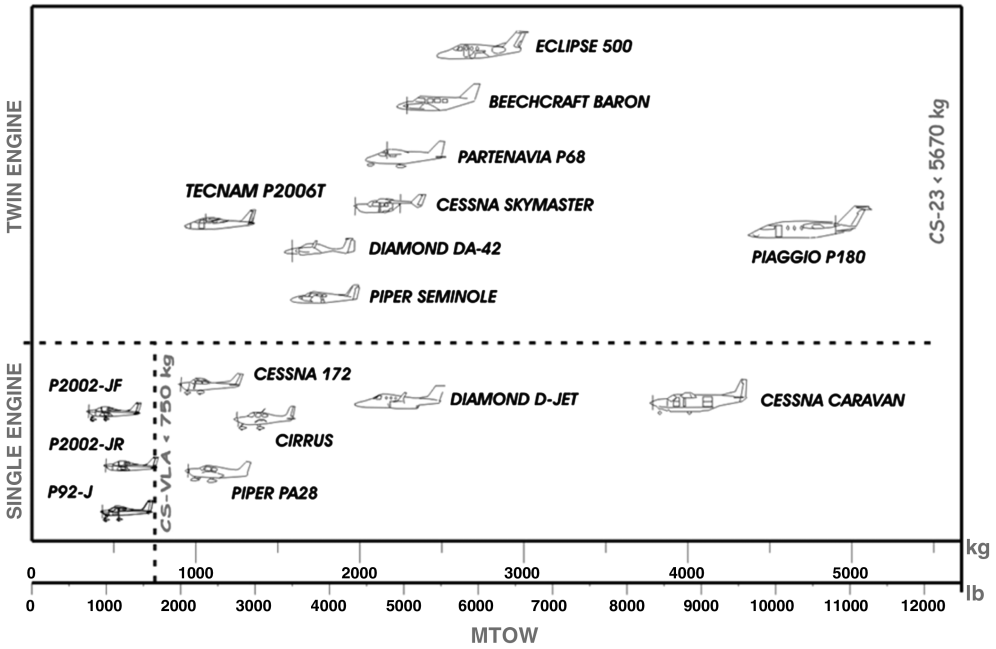

Fig. 3 Single- and twin-engine weight data. (Courtesy of Tecnam.)

a) **b)**

Fig. 4 Aircraft: a) cockpit and b) baggage compartment.

Fig. 6) and allows the measurement of the angle of attack and the angle of sideslip with an accuracy of about 0.20 deg.

Particular care has been taken in mounting a load cell on the control stick in order to measure the piloting effort (Fig. 7), which has also been useful for static stability demonstration. A set of potentiometers has been installed on the aircraft to measure the deflection of control surfaces (Fig. 8) with an accuracy of about 0.2 deg.

A very accurate inertial measurement unit (XBow AHRS 400) has been used to measure angles, accelerations, and angular rates, and it has been located close to the aircraft X_{cg} [average position 25% of the mean aerodynamic chord (MAC)]. The accuracy of the measurement of the angles, angular rates, and accelerations are, respectively, 0.5 deg, 0.3 deg /s, and 0.03 g. Concerning the static measurement of the angles, the inertial platform has been also calibrated in our laboratory using a digital inclinometer with an accuracy of 0.1 deg. The angle calibration in dynamic conditions has not been performed, and the calibration given by the XBOW factory has been used. However, the AHRS-400 inertial platform is characterized by an automatic erection rate that improves the accuracy in the dynamic condition with respect to the previous model. All flight tests have

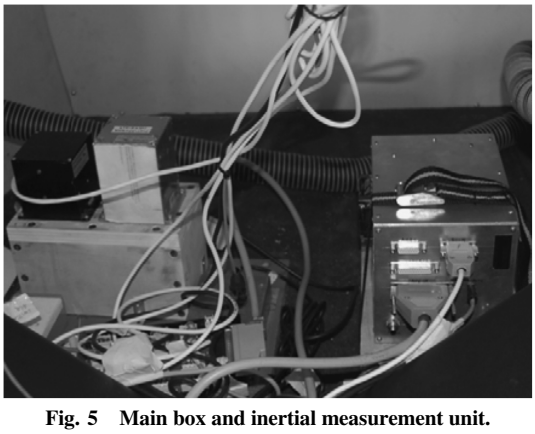

Fig. 5 Main box and inertial measurement unit.

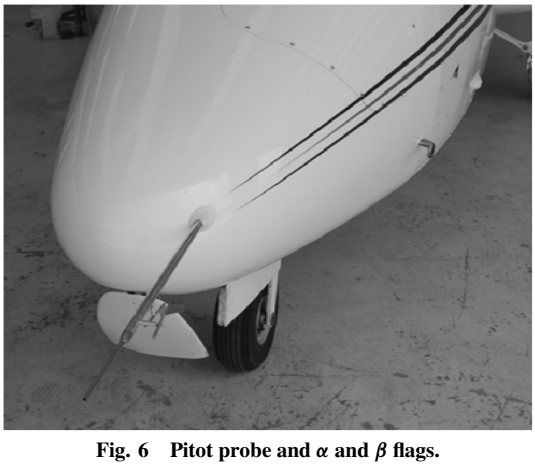

Fig. 6 Pitot probe and α and β flags.

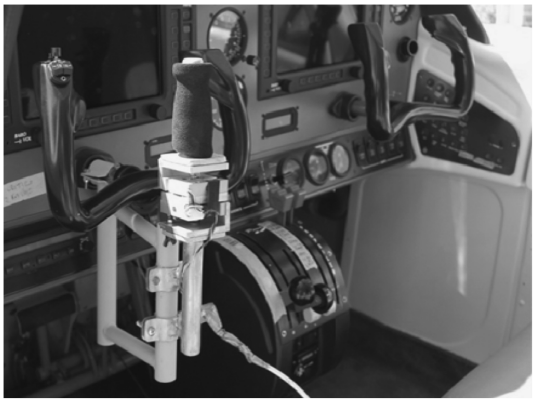

Fig. 7 Load cells for stick force measurements.

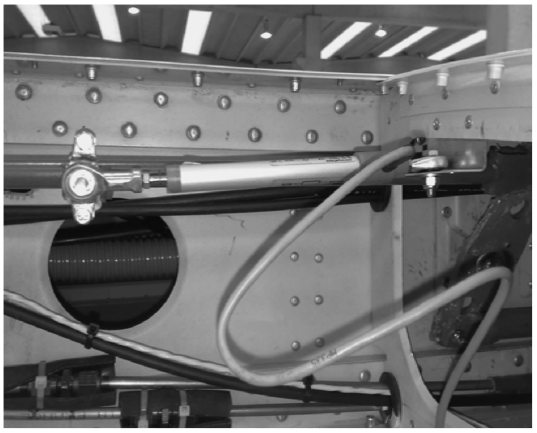

Fig. 8 Position transducer: aileron control.

been performed with a 10 Hz sampling rate. The system is also equipped with a dual-frequency GPS for position and GS measurements. The GPS is acquired simultaneously with the other flight data and with a sample rate of 10 Hz.

Before the flight tests, the whole instrumentation has been subjected to a thorough calibration phase. In particular, the mini-air data boom has also been calibrated in the wind tunnel of the DIAS (Fig. 9), while the pressure sensors and load cells were calibrated in the same laboratory (Fig. 10). All installed potentiometers have been calibrated during the their installation, using a tool of the CSYS.

IV. Flight-Test Performances

Flight tests addressed to flight-performance measurement have been carried out in order to complete flight certification and in order

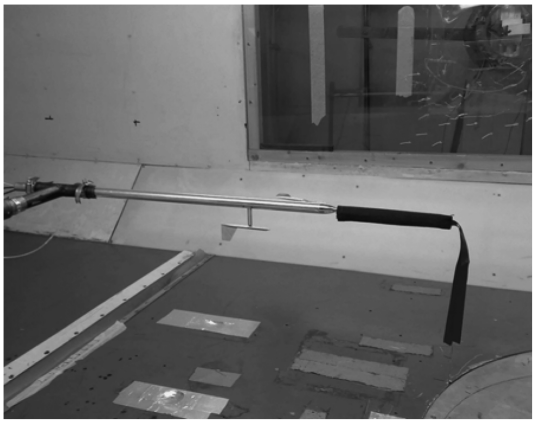

Fig. 9 Wind-tunnel mini-air data boom calibration.

Fig. 10 Load cells calibration.

to release an official version of an aircraft flight manual. As already outlined in Sec. I, the measurement flight performances have been fundamental in the preliminary setup of the first prototype. The aircraft has been slightly improved during the first months, after preliminary flight tests. An example is the wingtip modification with the design of the winglet to improve the OEI RC [19,20]. Flight tests have also been crucial to tune all onboard systems, electronic items, and hydraulic/electrical systems, like the landing-gear retraction system. Many of these tests have been also crucial for CS-23 aircraft certification.

A. Pitot-Static System Calibration

The purpose of the calibration is to reveal the position error of the airspeed pitot-static system installed on the airplane. The dynamic pressure measured through the pitot probe described in Sec. III has also been recorded, and this system, mounted on the nose of the aircraft, has shown negligible error when compared with the calibrated speed. However, the following results show the error of the airplane factory pitot-static system, composed of two pitot probes installed on both sides of the aircraft nose and static ports located on both sides of the fuselage below the wing.

The method used to calibrate the pitot-static system is the speed-course method together with GPS measurements [1,10–12,21]. A series of courses over a base of known length (the measured base, in our case, measuring about 3 km) have been performed for the test; the errors due to the position of the pitot-static system are calculated by measuring the GS and evaluating the time necessary to perform two different courses (in opposite directions to cancel wind effects) on the measured base. Then it has been estimated as the true level flight speed. During the previously mentioned test, the wind speed was close to 10 kt and parallel to the direction of the chosen base. The aircraft weight W was 1180 kg and the c.g. position was at 20% of the MAC. The altitude maintained at each run was sufficient to allow the pilot to visually evaluate the initial and final times of each run and very close to sea level (S/L) (approximately 100–200 ft). The GS measured by the previous method (speed course) was always in good agreement (less than 1% difference) with the GS measured and recorded by the onboard GPS. Tests have been conducted with no atmospheric turbulence and with the following configurations and speeds.

Each course has been conducted, stabilizing the aircraft at the test speed and at the required configuration, before entering the measured base. The speed, elevation, and direction were kept constant. The airspeed system was calibrated in flight, and the related error was determined accordingly. The error was less than 5 kt in the range from $1.3V_{s1}$ to V_{NE}. The results are summarized in Table 6 and represent only part of the whole pitot-static system calibration.

The data shown are only the most representative, especially concerning cruise configuration. The data presented for takeoff and landing are only representative of one of the more accurate tests and show an acceptable error. The average GS, shown in Table 6, has

Table 6 Pitot-static system calibration, speed-course method, GPS measurements, and performed courses results

Map, Hg	RPM	Flaps, deg	Gear	OAT,a °C	Time, s	Average GS, kt	V_{CAS}, kt	V_{IAS}, kt	Error, %
21.3	4900	0	Up	9	65 78	83.2	84.1	80	5.1
24.7	5500	0	Up	9	54 46	119	120.3	120	0.3
29.8	5500	0	Up	9	46 38	142	143.5	145	−1.0
		Takeoff	Down	12	82 109	63	63.3	60	5.5
		Landing	Up	13	115 121	60.5	60.7	55	10.3

[a]OAT denotes outside air temperature.

been obtained through the course length and the times shown in the same table. Differences of this speed and the one acquired through the GPS of less than 0.3 kt have been observed.

Figure 11 shows the obtained pitot-static system calibration curve valid in all flight speed envelopes, accordingly to necessary flap deflection, and used for all flight performances, to transform indicated airspeed into the one calibrated.

B. Stall Tests

Stall performances of the P2006T aircraft are determined according to CS-23.49 and CS-23.201 [1]. The preliminary goal is to define when the airplane can be considered stalled for airplane certification purposes [1]. According to CS-23.201(b) regulations, starting from a speed at least 18.5 km/h (10 kt) above the stall speed, the elevator control must be pulled back so that the rate of speed reduction will not exceed 1 kt/s for leveled stall and 3 kt/s in turning stall. The possible stall conditions are 1) uncontrollable downward pitching motion; 2) downward pitching motion that results from the activation of a device (for example, a stick pusher); and 3) the control reaches the stop.

The stall requirements must be attained according to CS-23.201 in the following configurations: 1) MTOW; 2) engine running at 75% and idle; 3) flap retracted, takeoff (15 deg), and full-flap landing (40 deg); 4) landing gear retracted and extended; 5) trim speed ($1.5V_{S1}$); 6) c.g. in the maximum forward and aft positions; and 7) leveled stall and turning stall with 30 deg of bank.

More than 100 stall tests have been necessary to cover all the required combinations of the previously mentioned conditions to achieve the final certification.

Aircraft weight has a direct effect upon stalling speed. Stalling speed will increase as weight increases. In fact, the maximum lift coefficient should be almost constant, depending only on the aerodynamic configuration. The location of the aircraft center of gravity has a major effect upon stalling speed. Aft movements of the c.g. result in a reduction of the balancing (downward) tail load. This means that, with a certain lift generated by the wing, the aircraft lift coefficient (wing plus tail) will be higher, which results in a lower stalling speed. For this reason, it is necessary to perform the stall test with the c.g. in both the most forward position (critical for the reasons discussed previously) and the most aft position (critical for both longitudinal and directional controllability).

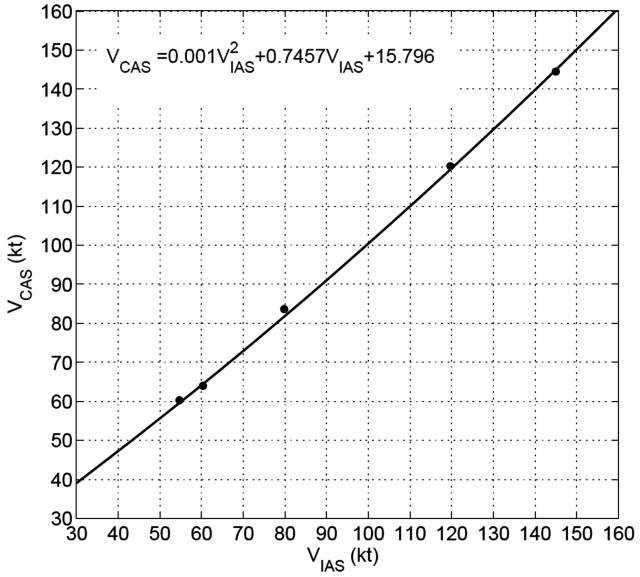

Fig. 11 Pitot-static system calibration curve.

Some typical time histories for a level stall are shown in Fig. 12. The tests have been performed at an altitude from the ground of about 2000 ft. The altitude shown in Fig. 12 is the pressure altitude recorded by the system and calibrated in ISA condition. The altitude should be considered, not as an absolute value, but only to show altitude variation during the test. It is possible to see that the ER is near 1 kt/s, as specified by certification rules. Moreover, the load factor in the correspondence of the stall (minimum flight speed) is less than one ($a_Z = 0.921$ g), and the value of the lift coefficient, called $C_{L\max}$ [see Eq. (1)] (obtained with both measured stall speed and measured load factor), is lower than the stall lift coefficient C_{Ls} [see Eq. (2)], obtained according to CS-23 with $a_Z = 1$ g. Many level flight stalls have been performed in all configurations and with maximum forward and aft c.g. positions. In all tests, particular attention has been paid to stall ER [11,12]. In Fig. 12, the difference in stall speed between the cruise configuration (Fig. 12a) and the full-flap landing configuration (Fig. 12b) is also clear. The leveled stall speed obtained is about 56 kt in cruise configuration and about 41 kt in full-flap landing configuration:

$$C_{L\max} = \left(\frac{a_Z W g}{(1/2)\rho V_S^2 S}\right) \tag{1}$$

$$C_{Ls} = \left(\frac{W g}{(1/2)\rho V_S^2 S}\right) \tag{2}$$

Figure 13 presents time histories of a turning stall (always with forward position of the c.g.) and of a leveled stall with a full flap and the c.g. in the maximum aft position (30% of the MAC). All performed stalls with the c.g. in the maximum aft position have shown more difficulties for the pilot to obtain and ER close to one and, for the reduced stability and consequent higher maneuverability, the aircraft enters into a deeper stall (see the angle of attack in Fig. 13b that is up to 30 deg just before stall). The stall (see again Fig. 13b) is also characterized by high values of the bank angle that, in poststall condition, are up to 50 deg in absolute value.

Table 7 shows some stall tests performed for aircraft certification. The certified stall speed in level flight (engine in idle condition) with a MTOW of 1180 kg is about 60 kt with the flap retracted and, respectively, 52 and 47 kt with the flap extended in takeoff (15 deg) and landing (40 deg) conditions. It can be observed that, for all stall tests reported and used for aircraft certification, the ER is always close to one and the load factor at stall is also slightly lower than one (between 0.85 and 0.95). The difference between the obtained stall lift coefficient and the maximum lift coefficient is very small.

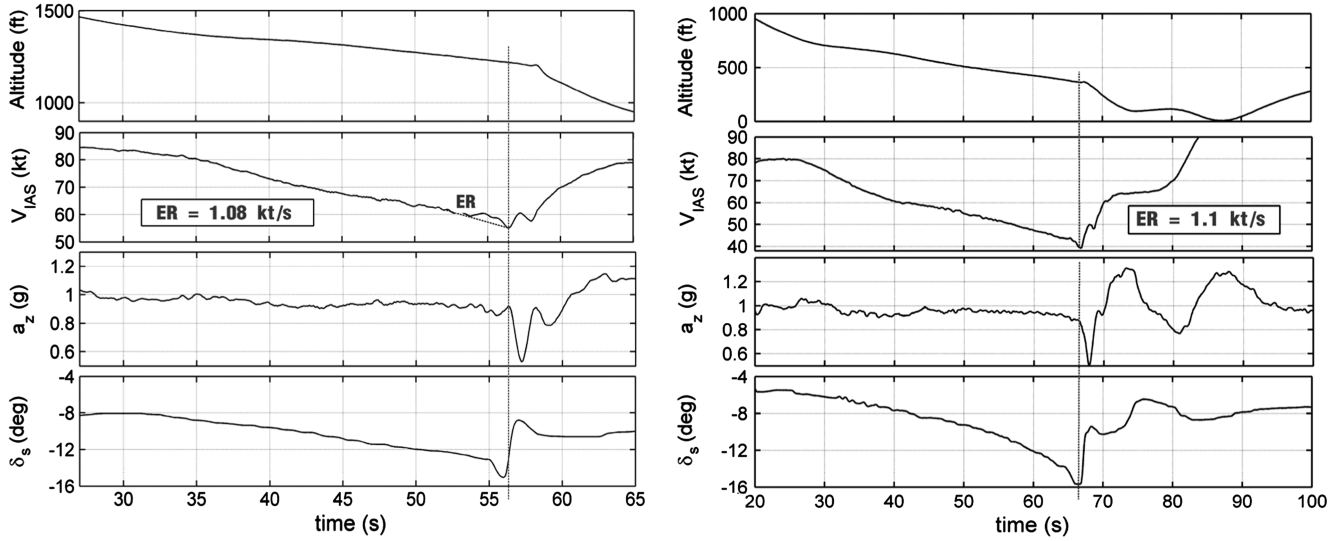

a) Leveled; flap 0 deg; X_{CG}/c = 16.5%

b) Leveled; flap 40 deg; X_{CG}/c = 16.5%

Fig. 12 Leveled stall a) with flap retracted and (b) with a 40 deg (landing) flap deflection. Both tests are with engine idle and maximum forward position of c.g.

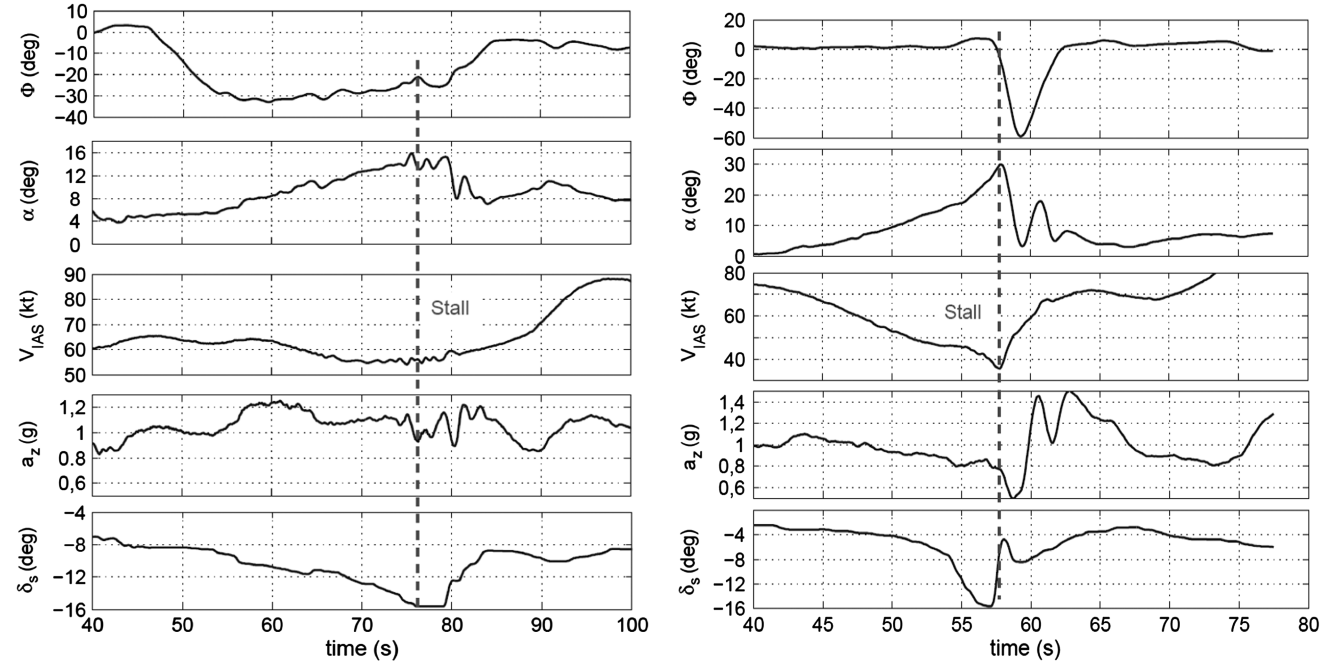

a) Turning; flap 0 deg; X_{CG}/c = 16.5%

b) Level stall; flap 40 deg; X_{CG}/c = 30%

Fig. 13 Turning stall a) with flap retracted, c.g. maximum forward, and level stall and b) with 40 deg flap deflection and c.g. maximum backward. Both tests are with engine idle.

Table 7 Results of some stall tests performed for certification

Type	Flap, deg	Landing gear	V_S, kt	a_z	ER,kt/s)	C_{Ls}, Eq. (2)	$C_{L\max}$, Eq. (1)
Stall tests c.g. max forward (16.5%)							
Leveled	0	Retracted	55.5	0.92	1.1	1.46	1.34
Leveled	0	Extended	60	0.92	0.8	1.26	1.16
Leveled	15	Extended	45.8	0.84	-	2.08	1.75
Leveled	40	Retracted	41.3	0.88	1.1	2.51	2.22
Leveled	40	Extended	43	0.84	0.7	2.33	1.97
Turn	0	Retracted	65.7	0.97	0.8	1.06	1.04
Turn	40	Retracted	54	1.14	0.5	1.75	1.53
Stall tests c.g. max aft (30.5%)							
Leveled	0	Retracted	55.2	0.93	2.7	1.47	1.38
Leveled	40	Retracted	47	0.89	1.9	1.98	1.78
Turn	0	Retracted	62	0.97	1.3	1.19	1.15
Turn	40	Retracted	53	0.97	2.5	1.59	1.54

Table 8 Stall tests performed at different ER with flap retracted and c.g. maximum aft

Test	X_{cg}/c, %	V_{IAS}, kt	V_{CAS}, kt	a_z, g	ER, kt/s	C_{Ls}	$C_{L\max}$
1	30.5	58.7	60.7	0.91	1.2	1.31	1.19
2	30.5	56.3	58.3	0.89	1.5	1.42	1.26
3	30.5	51.4	54	0.81	3.1	1.65	1.34
4	30.5	46.5	48.9	0.7	6	2.02	1.41

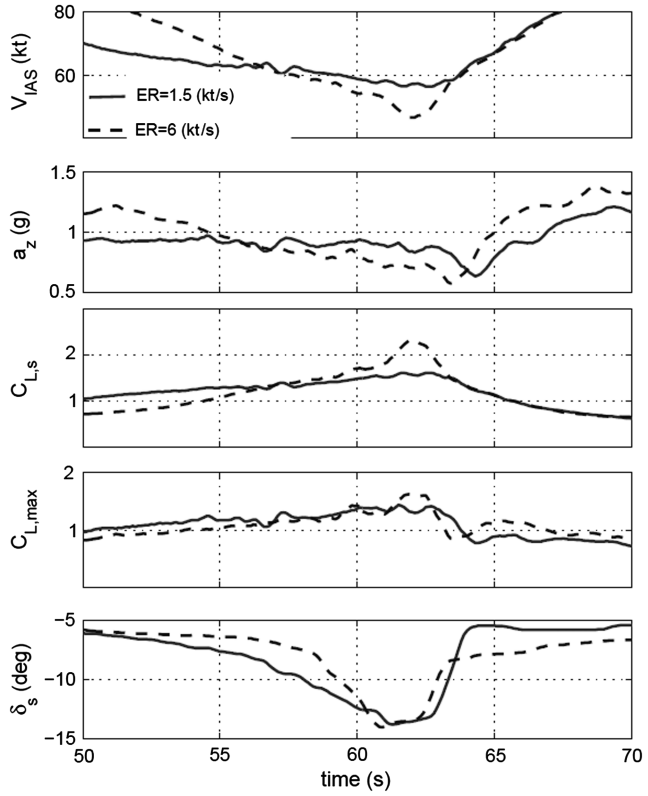

Fig. 14 Comparison of stall tests 2 and 4 of Table 8: flap retracted and c.g. maximum aft (30% of MAC).

Table 7 also shows that there is a small influence for the landing gear on measured stall speed (and stall lift coefficient). Looking at the results, for all flap deflections, the landing gear extracted causes an increase of stall speed of about 4 kt with the flap up and 2–3 kt with a full flap. The measured and averaged (four stall tests have been repeated for each configuration reported in Table 7) stall lift coefficients are about 1.45 with the flap retracted (cruise configuration) and 2.4 in the full-flap landing configuration. These values confirm the accurate aerodynamic design that has been accomplished for the high-lift system and for the wing stall characteristics, also in terms of stall path, as previously shown by Nicolosi and Pascale in [2,3].

However, the effect of the ER on the measured stall maximum lift coefficient C_{Ls} and the maximum lift coefficient with the effective load factor $C_{L\max}$ at stall in level flight and cruise (no flap) configurations has been the object of a deep experimental investigation and not focused on aircraft certification, but focused mainly on scientific purposes. In Table 8 are shown the results of some leveled stall tests performed in cruise configuration (flap retracted) and with the c.g. in the maximum aft position, with different maneuvers performed by the pilot and characterized by different ER values. It can be clearly observed that a higher ER leads to a lower stall speed and a higher difference between the previously mentioned lift coefficients, due to the lower load factor attained at stall.

Figure 14 shows the comparison between two time histories of two different stall maneuvers (tests 2 and 4 of Table 8). It can be observed that the higher ER (due to higher deceleration imposed by pilot maneuver, see stabilator deflection in Fig. 14) leads to a lower stall speed with a corresponding lower load factor. In Fig. 15, the results of the tests reported in Table 8 are plotted in terms of stall speed (Fig. 15a) and in terms of the stall lift coefficient and maximum lift coefficient (Fig. 15b). The symbols in the figure represent acquired data. It can be observed that the certified stall speed in the cruise configuration is about 59–60 kt and corresponds to a C_{Ls} value around 1.35. It is also interesting to observe that the influence of the ER (expressed in knots per second) is higher for C_{Ls} than for $C_{L\max}$. This is mainly due to the strong direct influence of the ER on the load factor at stall. It is also very interesting to see that extrapolating data at ER $= 0$ leads to a very close value for both lift coefficients and indicates a static maximum lift coefficient in cruise configuration and a flight Reynolds number of about 1.25.

C. Winglet Design

The first prototype of the aircraft used for flight tests with a weight of about 1100 kg was characterized by a wing span of 11.2 m, a wing area of $S = 14.74$ m^2, and an aspect ratio of AR $= 8.46$. Several tests

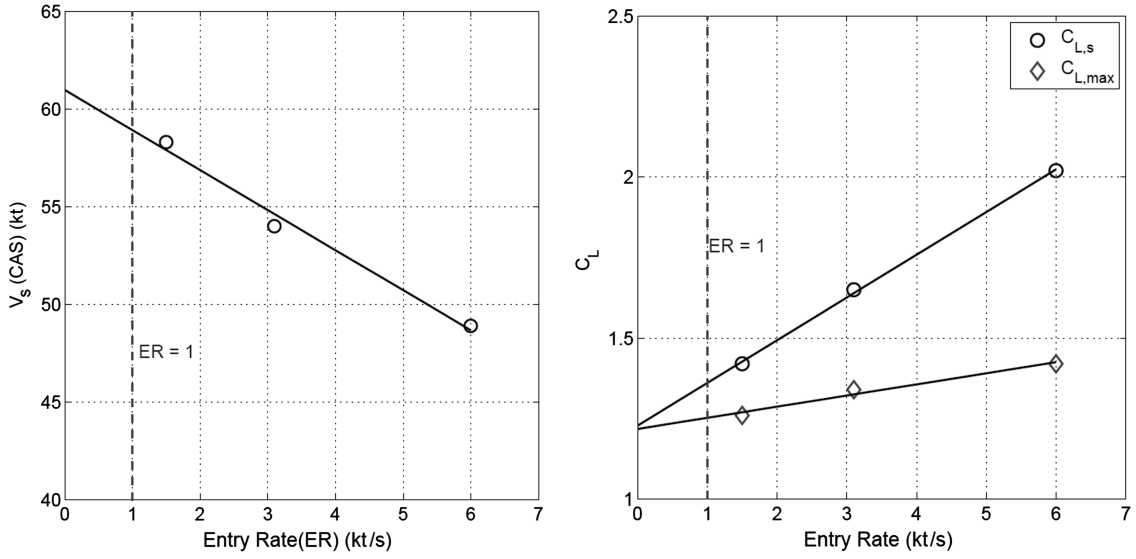

a) Stall speed vs entry rate **b) Stall lift coefficients vs entry rate**

Fig. 15 Leveled stall at different ERs, cruise configuration and c.g. maximum aft, and global results.

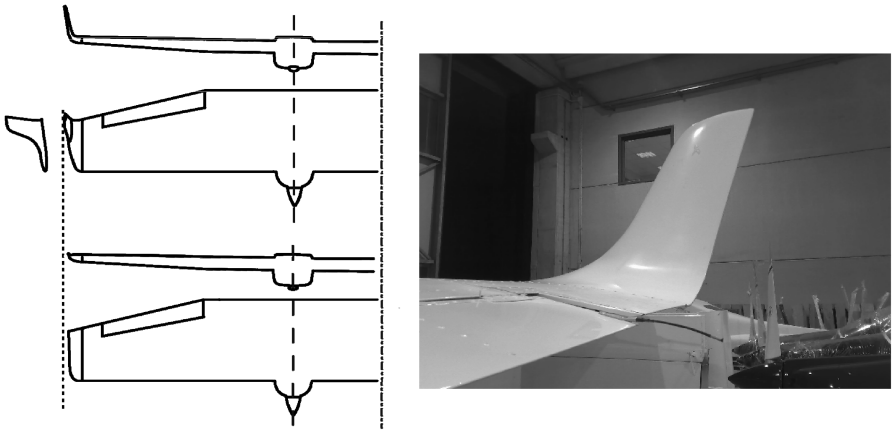

a) b)

Fig. 16 Aircraft: a) wing drawings before and after winglet design and b) picture of final designed winglet installed.

were performed to highlight level flight and climb performances. As also reported in Sec. IV.E, climb performances in OEI conditions were especially unsatisfactory, and it was decided to modify the aircraft wingtip by installing winglets. As also outlined in Sec. IV.E, the winglets (designed at DIAS by Nicolosi and Pascale [2], Nicolosi [19], and Coiro et al. [20]) were designed to increase the aircraft's induced drag factor with a very low penalty in level flight performances. The wing wetted area was maintained the same and, after winglet installation, the aircraft was characterized by an increased wing span (only 0.20 m higher; 11.4 instead of 11.2 m), about the same wing planform area (14.76 m^2), and an increased wing AR = 8.76 (see Fig. 16). Calculations performed in the design and optimization of the winglet (performed through the use of a panel method code) showed an increment of induced drag factor due to the winglet of about 0.09. In addition, wind-tunnel tests have been performed on a semimodel of an elliptical wing with the designed winglet installed [20], and a measured increment of the induced drag factor of 0.08 has been noticed. The winglet height was chosen to be about 10% of the wing semispan (0.6 m) and was limited to avoid an excessive increment of wing-bending moment at the root (the wing structure was not modified) and also to limit the aerodynamic load on the winglet and the weight of the winglet itself. The winglets were manufactured in composite material (as the wingtip of the original prototype) and installed on the aircraft (see Fig. 16), and the aircraft MTOW was modified and increased to 1180 kg. The aircraft's main geometrical parameters before and after winglet installation are summarized in Table 9. The estimated aircraft induced drag efficiency factor e, according to wind-tunnel tests performed on the aircraft scaled model with nacelles and calculations, is 0.72 for the aircraft without winglets and about 0.82 for the aircraft with winglets.

Calculations performed during winglet design and preliminary flight tests of the original prototype indicated that the parasite drag coefficient should be increased only a few drag counts due to the winglets. The final drag characteristics of the aircraft equipped with the winglets, as measured in flight, will be shown in detail in the next paragraph.

D. Level Flight Measurements and Drag Polar Estimation

The lift and drag characteristics of the airplane have been determined from a series of steady, level flight data points conducted at pressure altitudes between S/L and 1000 ft, as also suggested in [11,22]. The drag polar characteristics could also be obtained through aircraft parameter identification, as suggested in [23], but through more complex and extensive flight tests. Several level flight tests have been performed to measure the aircraft required thrust horsepower (THP) at different flight speeds. Engine brake horsepower (BHP) has been determined from engine manifold pressure, RPM, pressure altitude, ambient temperature, and using the power chart supplied by the engine manufacturer. In addition, the Rotax 912S engine has been tested in the laboratory of the Department of Mechanical Engineering of the University of Naples, and the engine manufacturer power chart has been slightly corrected. The power predicted from the engine chart has been also reduced to account for installation losses.

Therefore, THP has been determined from BHP, propeller RPM, air density, true airspeed (TAS), and standard NACA two-blade-propeller performance charts. The net installed propulsive efficiency η_p has been estimated using an empirical formulation based on the Society of British Aerospace Companies' standard method correction factors to account for nacelle blockage. The estimated net propeller efficiency (the previously mentioned correction lead to a value 4% lower than free air propeller efficiency) is between 0.7 (low speed) and 0.81–0.82 (high speed).

The weight has been determined for each point by taking into account the approximate fuel consumed. Drag characteristics were determined as follows. Assuming that drag can be represented by a standard parabolic drag polar,

$$C_D = C_{D_0} + \frac{C_L^2}{\pi \mathrm{AR} e} \tag{3}$$

then the parasite drag coefficient and the induced drag efficiency factor (also known as Oswald's efficiency factor) can be obtained through a plot involving the generalized velocity parameter VIW [see Eq. (4)] and the generalized power parameter PIW [see Eq. (5)] [11,22]. This is important to obtain some generalized data to be enveloped, starting from acquired data in different conditions of weight, temperature, and altitude. As the standard weight W_{std} has been assumed as the aircraft MTOW of 1180 kg,

$$\mathrm{VIW} = V\sqrt{\sigma \frac{W_{\mathrm{std}}}{W}} \tag{4}$$

$$\mathrm{PIW} = \mathrm{THP}_r\sqrt{\sigma\left(\frac{W_{\mathrm{std}}}{W}\right)^3} \tag{5}$$

Figure 17 shows the plot of (VIW, PIW) points collected through several flight tests performed on the aircraft configuration before and after winglet installation. The generalized power curve (PIW × VIW vs VIW^4) is also reported in Fig. 18 for the aircraft, with and without winglets. The slope and the intercept of this generalized curve readily give estimates of, respectively, the minimum drag coefficient and

Table 9 Geometrical characteristics and Aircraft weight before and after winglet installation

	b, m	S, m^2	AR	W_{TO}, kg
No winglet	11.2	14.74	8.46	1160
With winglet	11.4	14.76	8.76	1180

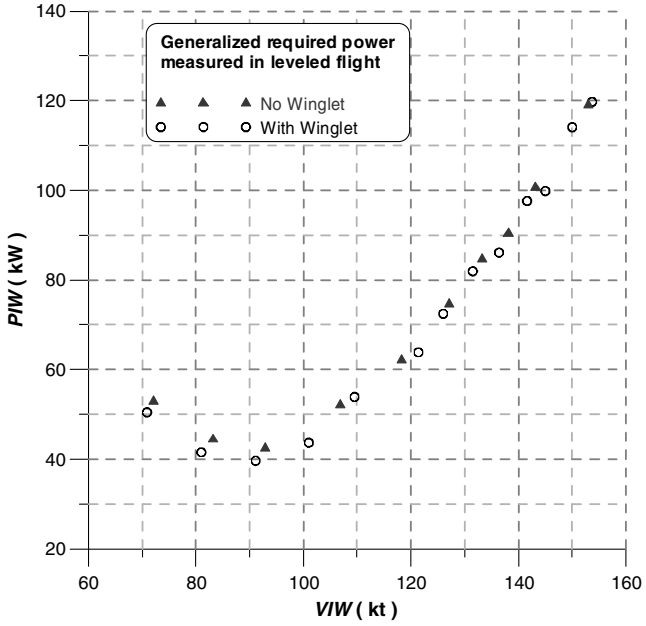

Fig. 17 Generalized velocity vs generalized power parameter, before and after winglet installation.

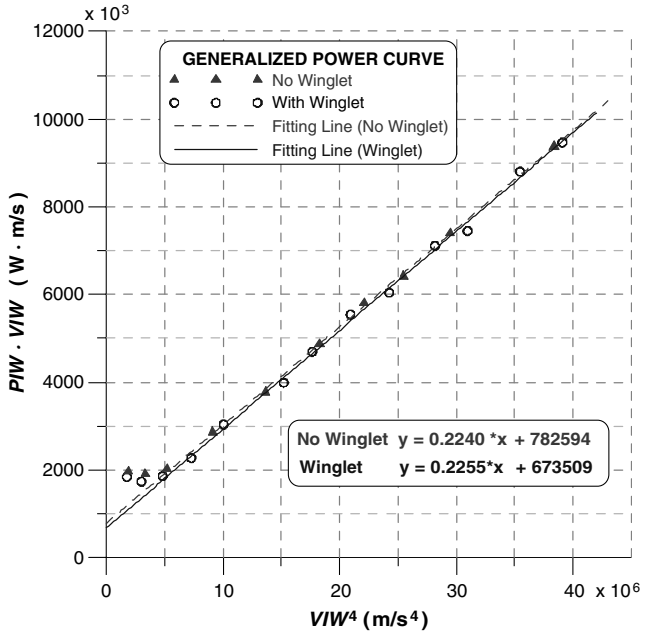

Fig. 18 Generalized power curve, before and after winglet installation.

Oswald's efficiency factor. Assuming a generic linear equation, as shown in Eq. (6), Oswald's efficiency factor has been estimated from Eq. (7) and the minimum drag coefficient has been estimated from Eq. (8):

$$y = A \cdot x + B \tag{6}$$

$$e = \frac{2W_{\text{std}}}{B\rho_0 S\pi \text{AR}} \tag{7}$$

$$C_{D_0} = \frac{2A}{\rho_0 S} \tag{8}$$

The obtained results from flight tests are summarized in Table 10. In the same table, we have reported the values of C_{D0} and e, calculated (estimated) on the basis of wind-tunnel tests [2,3] performed on a scaled model (without winglets) of the aircraft at a low Reynolds number (0.6×10^6) appropriately corrected for the flight Reynolds number (about 4×10^6). Wind-tunnel test measurements [2,3] gave a value of Oswald's efficiency factor for the configuration with no winglets (but with nacelles) equal to about 0.72. The corrected value for the parasite drag coefficient, including the estimated additional items (such as cooling drag), was 0.0258. As already outlined in the previous paragraph, the effect of winglets on both coefficients has been estimated through the use of a panel method computer code, and the induced drag gain has also been measured by testing, in the wind tunnel, the designed winglet installed on a semimodel of the elliptical wing [20]. Before the flight tests, the expected increment of the parasite drag coefficient due to the winglets was estimated to be two drag counts (leading to a parasite drag coefficient of 0.0260 for the aircraft equipped with the winglets), and the estimated induced drag efficiency factor was 0.82. All the estimations are in good agreement with the final values measured through the flight-test procedure described previously. Because of the winglets, the final flight-measured value of e is equal to 0.80, confirming the expected increment estimated in the design phase.

Table 10 also shows that the use of winglets leads to an increase of the effective aspect ratio ARe (AR $\times$ e) of about 17% (from 6.0 to 7.0). A global lift-dependent drag reduction of about the same amount has to be expected. As the wing is characterized by the same wetted area, the winglet has been designed in such a way to avoid any decrease in aircraft flight maximum leveled speed. The lift coefficient in cruise condition is higher than zero, and the reduction (due to the winglets) of lift-dependent drag is higher than the previously mentioned parasite drag increase of two counts. Therefore, due to this global gain in drag, winglet installation has also led to an increase of cruise speed (75% of throttle setting, 7000 ft) of about 2 kt. A very small gain (about 1 kt) in maximum level speed at S/L (full power) due to the winglets has been also observed and reported in Table 10.

E. Climb Tests

In a preliminary phase, some climb tests in the OEI condition have been performed. The first aircraft prototype used for flight tests with no winglet was characterized by a wing span of 11.2 m. The first tests of the OEI climb at S/L and MTOW showed an OEI maximum RC of about 190 ft/ min (at standard ISA conditions). This is an acceptable RC, also compatible with the CS-23 aircraft certification [1], but it was not assumed such a good performance for the commercial success of the aircraft when also considering the possibility for the twin engine to operate in regions characterized by high temperatures (hot conditions) or high altitudes. These climb capabilities led the Tecnam design office modifying the wingtips and installing the winglets.

As highlighted in Sec. IV.C, after several months of research activity performed by Nicolosi and Pascale [2], Nicolosi [19], and Coiro et al. [20] at the University of Naples DIAS, the winglets for the P2006T have been designed (also with the help of several wind-tunnel tests [20] performed). The induced drag factor gain (from 0.72

Table 10 Geometrical and aerodynamic characteristics before and after winglet installation

			C_{D0}		Oswald factor, e			
	S, m^2	AR	Estimated	Measured flight test	Estimated	Measured flight test	ARe	Max lev. speed, kt
No winglet	14.74	8.46	0.0258	0.0248	0.72	0.71	6.0	153
With winglet	14.76	8.76	0.0260	0.0249	0.82	0.80	7.0	154

Table 11 Results of OEI climb tests with and without winglet

Test	Average V_{CAS}, kt	Reference pressure alt. hp, ft	RC corrected[a], ft/ min
Flight test: climb without winglet, W = 994 kg			
1	69.5	800	156
2	75	800	168
3	80	800	159
Flight test: climb with winglet, W = 1046 kg			
1	69	800	280
2	75	800	300
3	82	800	290

[a]Corrections have been applied with respect to weight (standard weight, WTO = 1180 kg) and standard atmospheric conditions (temperature and pressure), as suggested in literature [11,12].

to 0.80) and the small increment of geometric aspect ratio (8.46 to 8.76) due to the winglets should give a significant improvement of aircraft climb performance, especially in OEI conditions.

After winglet installation, OEI climb tests have been repeated, and the OEI maximum RC was measured. The results are summarized in Table 11. Figure 19 shows time histories of the OEI climb before and after winglet installation. The winglets have determined a noticeable increase of climb characteristics in OEI conditions. The maximum RC increased from 170 to 300 ft/ min. A maximum OEI RC at ISA, S/L, and a MTOW (1180 kg) of about 350 ft/ min has been extrapolated from flight tests. The winglets have determined such a dramatic improvement in the climb characteristics in OEI conditions

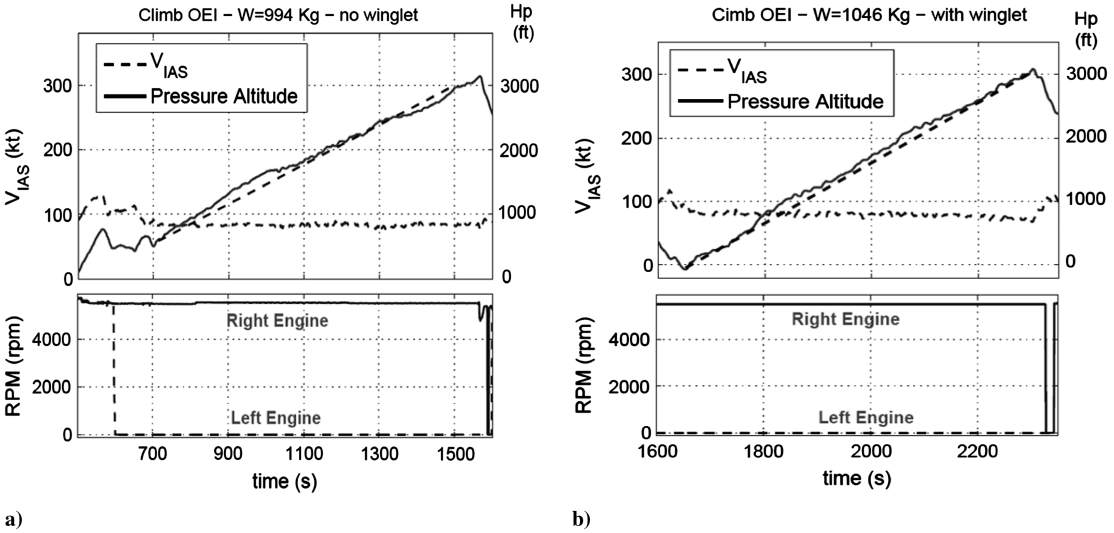

a) b)

Fig. 19 OEI climb of the aircraft a) before winglet installation and b) after winglet installation.

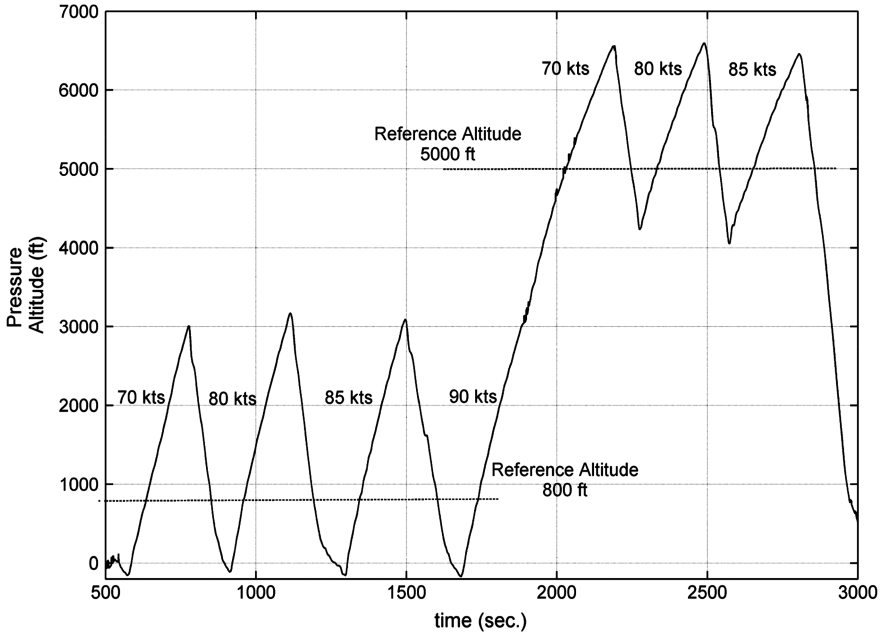

Fig. 20 Time histories of AEO sawtooth climb tests. Pressure altitude versus time.

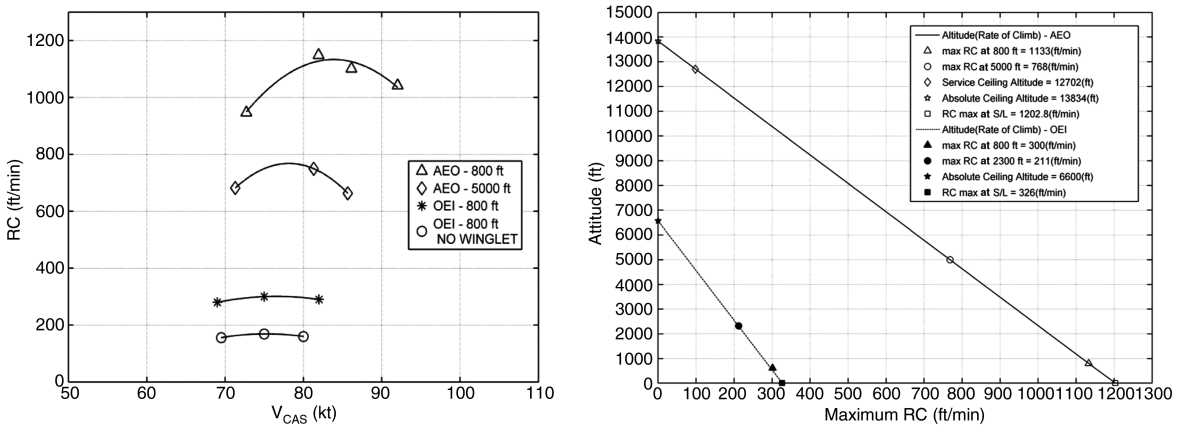

a) b)

Fig. 21 RC: a) flight measured versus speed and b) maximum versus altitude.

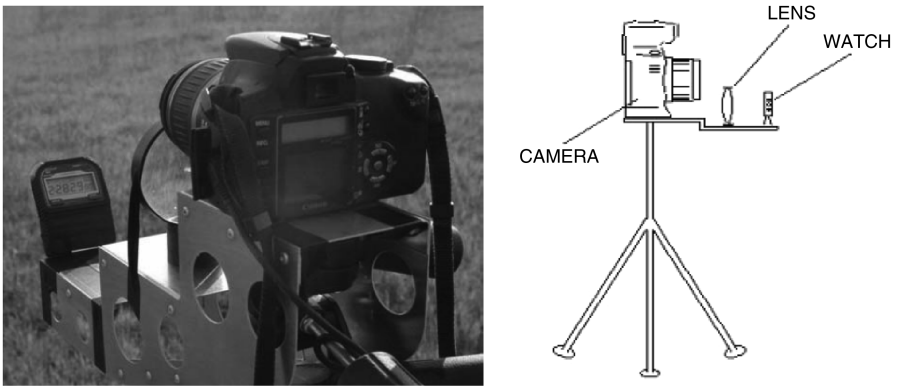

a) b)

Fig. 22 Camera: a) photo and b) drawing of camera, lens, and watch used for takeoff measurement.

that the maximum OEI RC has increased from 170 to 300 ft/ min; that is an increase of about 76%. Therefore, the use of winglets has become one of the key factors for aircraft commercial success.

The evaluation of climb performances in AEO of the P2006T has been carried out using the well-known sawtooth climb procedure [10–12], also according to the Federal Aviation Administration advisory circular 23-8B [24]. This test has to be performed in calm air, and it starts with the airplane in level flight, with the c.g. in the most unfavorable position. The procedure requires one of the following two situations: a climb of 3 min. or a change in altitude of 3000 ft. In each of our trials, we have prescribed four climbs, starting from a reference altitude of few feet, followed by three climbs,

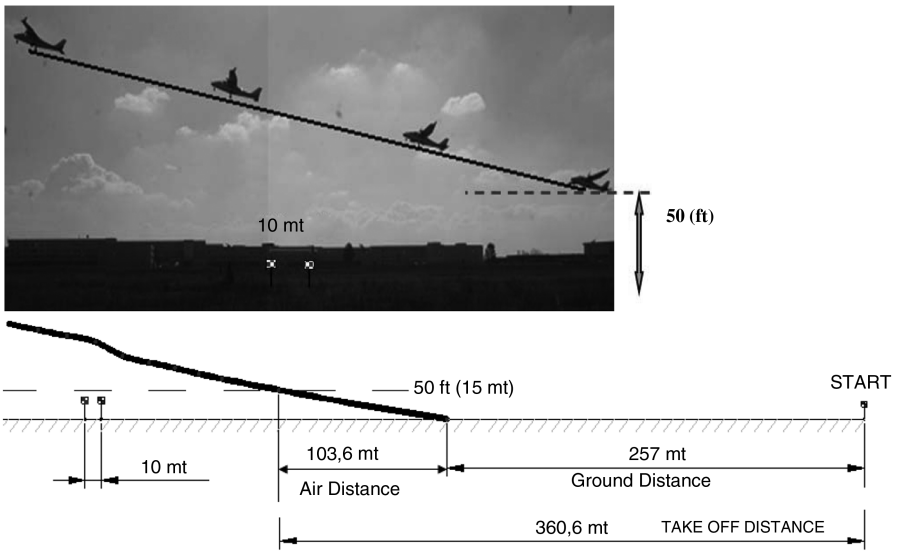

Fig. 23 Takeoff path reconstruction from pictures obtained by the camera.

Table 12 Results of takeoff tests

Takeoff number	Ground distance observed, m	Air distance observed, m	Total distance observed, m	W_{max}, kg	W_{test}, kg	OAT, °C	Relative air density σ	Ground distance corrected, m	Air distance corrected, m	Total distance corrected, m
1	257.10	103.60	360.70	1180	1185	17	1.013	260.61	105.01	365.62
2	269.50	93.38	362.88	1180	1184	17	1.013	273.78	94.86	368.64
3	276.30	84.50	360.88	1180	1183	17	1.013	281.30	86.03	367.33
4	305.73	84.65	390.38	1180	1182	17	1.013	311.95	86.37	398.32
5	322.50	80.83	403.33	1180	1181	17	1.013	329.79	82.66	412.44
6	303.80	75.25	379.05	1180	1180	17	1.013	311.35	77.12	388.46
Mean	289.16	87.04	376.20					294.80	88.68	383.47
Standard deviation	25.22	10.04	17.88					26.78	9.87	19.41

Table 13 Results of takeoff tests and recorded flight speed

Takeoff number	V_R, kt	V_{LOFF}, kt	V_2, kt
1	57.4	57.8	65.5
2	57.2	58.7	63.2
3	58.2	59.1	61.1
4	56.3	58.5	61.3
5	56.3	60.1	61.2
6	56.4	60.1	61
Standard deviation	0.77	1.77	2.77
Mean	56.97	58.95	62.22

starting from about 4000 ft. For each climb, we have acquired and processed the variation of pressure altitude. An example of pressure altitude time history for a test with AEO is shown in Fig. 20.

The climb rate determined with this test procedure has to be corrected [21,11,12] with standard corrections.

The standard weight used for weight corrections is the aircraft MTOW $W = 1180$ kg. The final RC at each flight speed obtained from the analysis of the data plotted in Fig. 21 and in conformity with standard conditions at a reference altitude of 800 and 5000 ft is plotted in Fig. 21a. The correction with respect to the weight has been applied, taking into account both direct correction [with certain excess power, the RC is inversely proportional to the aircraft weight] and correction due to the effect of the weight on lift-dependent drag (and required power). In Fig. 21b, the maximum RC versus the altitude is plotted, and the measurements of the service and absolute ceiling can be obtained with some approximation due to the lack of data at high altitudes. Other tests performed by the factory, and not available to the authors, have confirmed a service ceiling of about 13,000 ft. The maximum RC in the AEO condition, MTOW, and standard conditions is about 1200 ft/min. The aircraft service ceiling is about 12,700 ft (see Fig. 21b). Figure 21a also shows the RC in OEI conditions measured before and after winglet installation.

F. Takeoff Tests

Takeoff performances can ideally be divided into two phases: a ground phase (ground distance) and an airborne phase (air distance). The purpose of the test is to estimate the takeoff distance and a series of speeds according to regulations [1,21]. For the analysis of takeoff and landing, we have used the strip camera method: some observers are placed along the runway in order to assess the main points of the maneuver on the ground while the flight path is reconstructed using a dedicated digital camera, which is located at a known point on the runway (visual markers are used to refer the airplane's trajectory to the ground). The wind speeds during the tests were well below the maximum allowable (10 kt) and approximately 1 kt. All observed distances have been corrected for the effect of the wind speed. Figure 22 shows a picture of the camera used and a drawing of the camera with the lens and a watch to synchronize recorded data onboard the aircraft with the observed position by the camera.

An example of the takeoff path reconstruction is shown in Fig. 23. The measured flight path is also in good agreement with the aircraft position acquired through the GPS.

Six takeoff tests were conducted, and the results are reported in Table 12 and 13. The corrected values are obtained through standard correction procedures [12] for weight, temperature, and wind speed. The corrected average total takeoff distance (at ISA and MTOW) is about 383 m (with an average ground distance of 295 m).

Figure 24 shows a typical plot of acquired flight data during takeoff tests. In the same figure the values in correspondence of the aircraft rotation, liftoff, and passage over the 50 ft obstacle are indicated. In the figure, the pressure altitude also shows negative values after aircraft rotation; this is mainly due to the increase in static pressure observed by the two static ports just after rotation. The abnormal behavior of acquired pressure altitude (Hp) in the first 5 s is probably due to the effect of the acceleration (just after brake release) on the pressure transducers. The amount of necessary stabilator deflection to rotate the aircraft with the maximum forward (most critical) c.g. position is quite large (about -14 deg) and close to the final stop (about -17 deg).

G. Landing Tests

Landing performances have been evaluated with a procedure that is similar to the one used for takeoff [11,12]. The landing maneuver is also subdivided in an airborne phase (covering the air distance) and an onground phase (covering the ground distance). The same method with camera images has been used. Figure 25 shows the landing flight-path reconstruction. For landing tests, the wind speed was about 5–6 kt and has been carefully taken into account to obtain the corrected landing distance. Also for landing, six different tests had been performed. Tables 14 and 15 show results in terms of landing distances and landing speeds. The measured landing distance at MTOW (1180 kg), S/L, and ISA conditions is about 380 m.

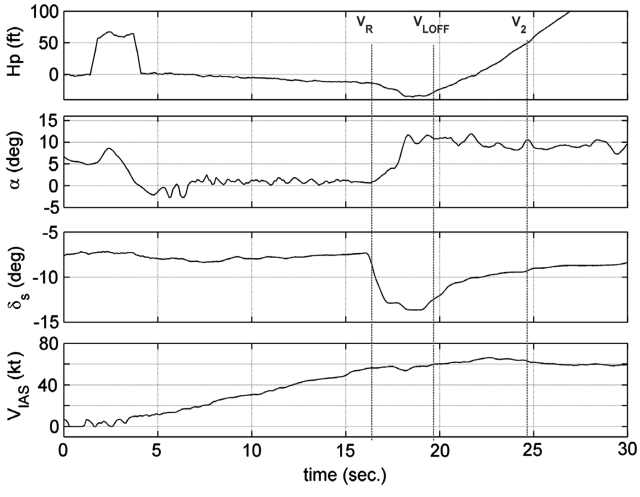

Fig. 24 Flight data acquired during takeoff 1.

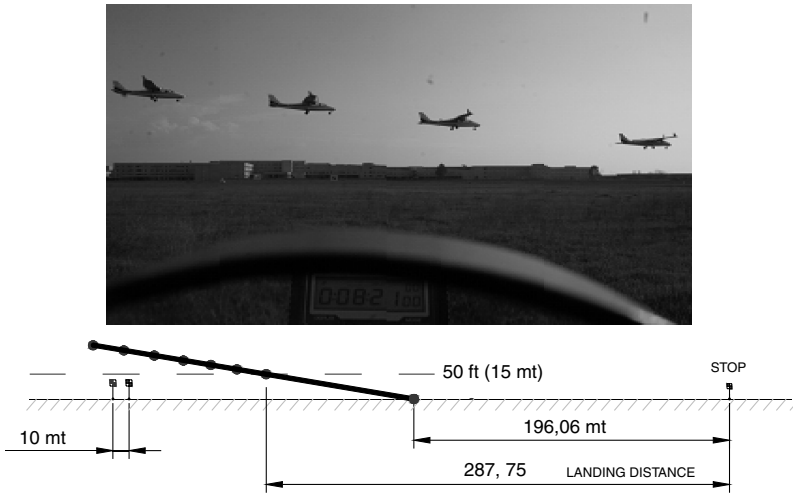

Fig. 25 Landing path reconstruction from pictures obtained by the camera.

The observed descent gradient (see Table 15) has never been very low (about 5 deg) but always safe and compatible with aircraft certification.

V. Stability and Flight Quality

The analysis of aircraft stability and of flight qualities has been carried out according to the regulation requirements. For these tests, load cells have been used to measure the stick forces. The results discussed next show the stable behavior of the airplane.

A. Static Longitudinal Stability

The static longitudinal stability test for this type of airplane must demonstrate that, starting from a trimmed flight condition, when the pilot applies a pulling or pushing force to the longitudinal control and then releases the stick slowly, the airplane finally returns in a trimmed condition, with a margin of 10% on the initial equilibrium speed. Besides, according to CS-23 [1], it must be demonstrated that "a pull must be required to obtain and maintain speeds below the specified trim speed, and a push required to obtain and maintain speeds above the specified trim speed." Figure 26 shows the maneuver performed to demonstrate aircraft static stability during a climb. When a trimmed condition is established, the pilot applies a pulling to the longitudinal control and then releases the stick slowly. During the climb, a tolerance of 10% on the speed is accepted, and the average TAS is 76 kt.

The aircraft neutral point and static stability can be established through flight tests with a standard method based on the measurement of stabilator deflections or through parameter estimation, as suggested in [25]. In our case, the aircraft static stability margin has been measured according to the methodology reported in [11,12]. Through establishing several level flight conditions, the stabilator deflections and flight speeds have been simultaneously acquired and recorded. Flight tests have been conducted at different positions of c.g.. Figure 27a shows the obtained results. The analysis of Fig. 27a, according to the technique suggested by Kimberlin [12], allows the measurement of a stick-fixed neutral point at different flight speeds, as shown in Fig. 27b. The neutral point position in cruise condition ($C_L = 0.50$) is located at about 43% of the reference MAC and is in good agreement with wind-tunnel measurements [3]. The neutral

Table 14 Results of landing tests and the landing distances

Landing number	Air distance observed, m	Ground Distance observed, m	Total Distance observed, m	W_{max}, kg	W_{test}, kg	OAT, °C	σ_{test}	Air Distance corrected, m	Ground Distance corrected, m	Total Distance corrected, m
1	91.69	196.06	287.75	1180	1180	18	0.990	188.27	239.52	427.79
2	91.15	188.30	279.45	1180	1179	18	0.990	168.39	227.28	395.67
3	83.90	180.30	264.2	1180	1178	18	0.990	161.34	218.71	380.05
4	89.28	151.90	241.18	1180	1177	18	0.990	147.34	183.39	330.73
5	99.65	196.70	296.35	1180	1176	18	0.990	157.83	240.23	398.05
6	73.11	190.30	263.41	1180	1175	18	0.990	150.10	232.02	383.02
Mean	88.13	183.92	272.06					162.21	223.53	385.89
Standard deviation	8.94	16.79	19.91					14.87	21.24	31.89

Table 15 Results of landing tests and the landing speeds

Landing number	V_{REF}, kt	V_{TD}, kt	Time from obstacle to touchdown, s	Descent gradient, deg
1	61	54	15	4.56
2	61	58	12	5.10
3	62	57	12	5.34
4	63	59	9	5.83
5	63	56	9	5.45
6	63	57	12	5.69
Standard deviation	0.98	1.72	2.26	5.33
Mean	62.17	56.83		

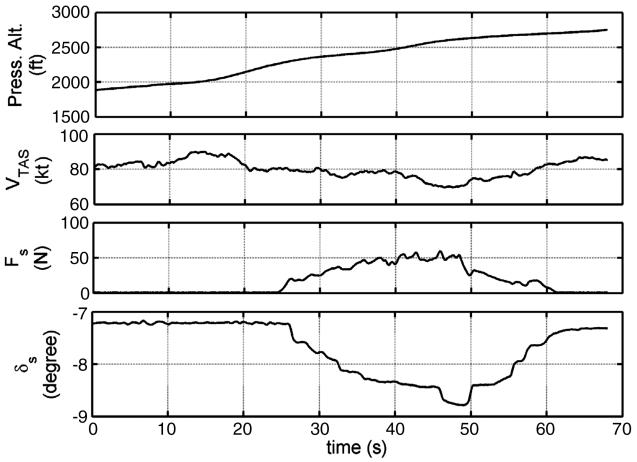

Fig. 26 Static longitudinal stability test (time histories).

stability point at 52% of the MAC for a lift coefficient of 0.75 can be observed from Fig. 27b.

Anyway, with respect to the cruise condition data measured, the other two lift coefficients examined (0.75 and 0.25) seem to lead to less reliable results due to the lack of data at high speed for $X_{cg}/c=30$. However, the higher slope $d\delta_s/d\alpha$ (higher static margin) at higher lift coefficients can be clearly observed in Fig. 27a. This is the well-known pendular stability effect, also observed during wind-tunnel tests, and it is due to the low position of the c.g. with respect to the wing chord, where aerodynamic loads are applied.

B. Static Lateral-Directional Stability

A significant amount of information concerning the aircraft lateral-directional stability characteristics is obtained by measuring the deflection of control surfaces, the piloting efforts, the angle of sideslip, and the angle of bank when the airplane is kept in flight in steady yawed flight.

Figure 28 shows that the airplane is statically stable both laterally and directionally. Figure 28a clearly indicates a positive directional stability of the aircraft. Figure 28b shows that, for positive sideslip

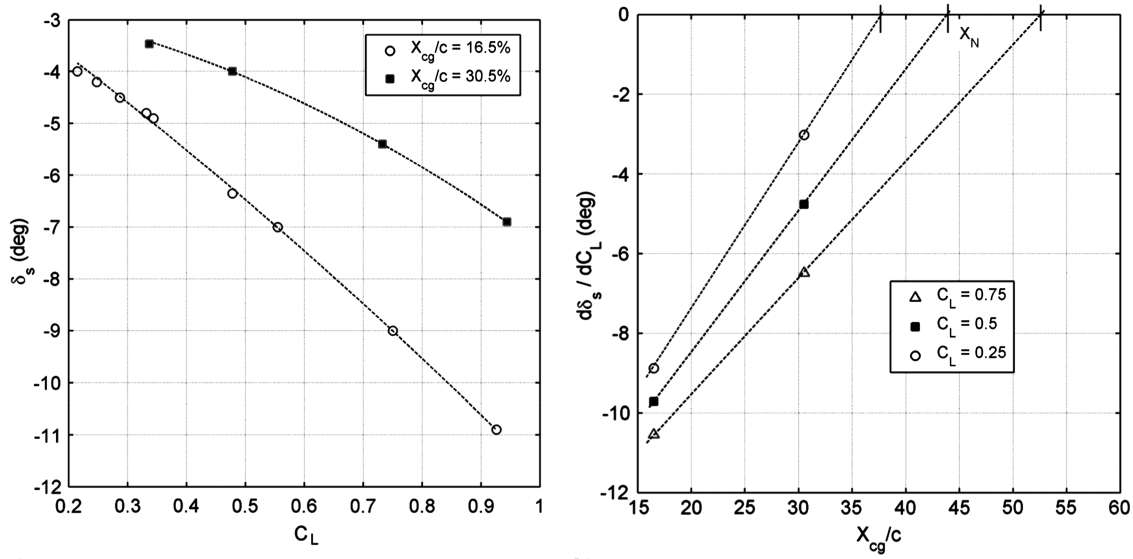

a) b)

Fig. 27 Flight static stability tests: a) required stabilator deflections versus life coefficient in level flight and b) stick-fixed neutral point estimation.

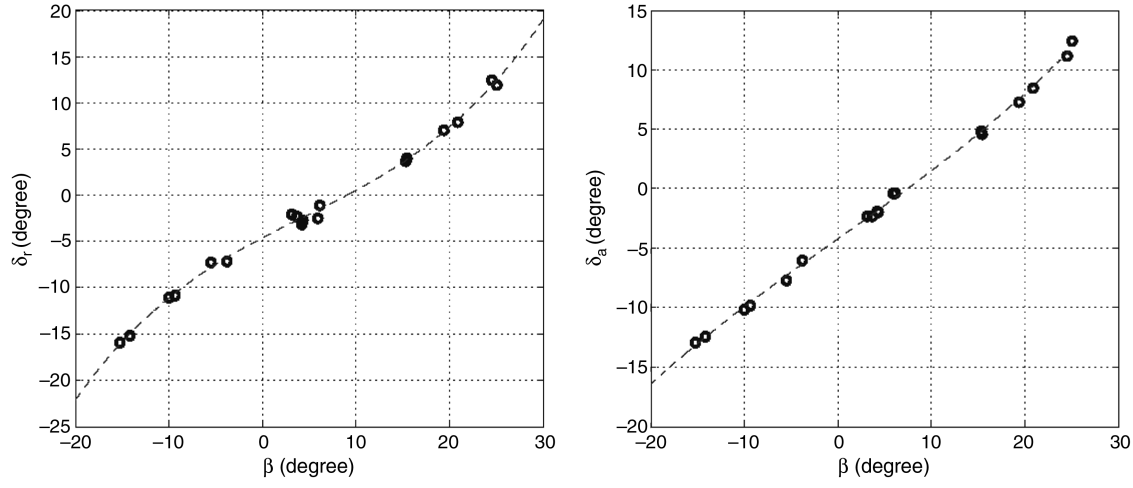

a) b)

Fig. 28 Demonstration of static lateral and directional stability–steady heading sideslip: a) rudder deflection and b) aileron deflection.

angles, it is necessary to compensate with right aileron downward deflections to avoid the rolling motion.

VI. Conclusions

The P2006T aircraft has been extensively tested in flight. The aircraft shows good flight characteristics and good flight performance. Flight tests have been successful for the aircraft certification released by the EASA in May 2009. The aircraft static and dynamic stability characteristics have also been measured. The aircraft exhibits good flying qualities. All the data measured during the wind-tunnel test campaign and during the flight-test activities, together with all numerical analyses (both aerodynamics calculations and flight dynamics simulations) represent a significant database for this twin-engine aircraft and can be extensively used for future tuning of numerical tools. Significant results have been obtained for the winglet effect on the OEI RC improvement.

The extensive and rigorous flight-test campaign carried out beyond certification requirements can contribute to the increase of confidence and safety in this aircraft and can be of great value as a database for a future similar design.

Acknowledgments

The authors wish to thank the Tecnam technical office for the research cooperation and technical support during the flight-test campaign. They also thank L. Pascale for his excellent design that has allowed very useful and interesting flight tests and collection of important scientific results.

References

[1] "Certification Specifications for Normal, Utility, Aerobatic and Commuter Category Airplanes," European Aviation Safety Agency CS-23, Koeln, Germany, 2003.

[2] Nicolosi, F., and Pascale, L., "Design and Aerodynamic Analysis of a Light Twin-Engine Propeller Aircraft," XXVI ICAS Conference, International Council of the Aeronautical Sciences Paper 2008-1.2.2., Stockholm, Sept. 2008.

[3] Pascale, L., and Nicolosi, F., "Design of a Twin Engine Propeller Aircraft; Aerodynamic Investigation on Fuselage and Nacelle Effects," *Aerotecnica Missili e Spazio*, Vol. 87, No. 3, July–Sept. 2008, pp. 99–114, http://www.aidaa.it/3-2008/P2006_corr.pdf [retrieved 25 March 2010].

[4] Coiro, D. P., Nicolosi, F., De Marco, A., and Familio, R., "Flight Test on Ultralight Motorglider, Aerodynamic Model Estimation and Use in a 6DOF Flight Simulator," *Aerotecnica, Missili e Spazio*, Vol. 87, No. 1, 2008, pp. 3–13, http://www.aidaa.it/1-2008/coiro.pdf [retrieved 25 March 2010].

[5] Giordano, V., Coiro, D. P., Nicolosi, F., Oliviero, P., De Marco, A., and Genito, N., "Light Aircraft Flight Tests: Performances, Stability and Flying Qualities Measurement," *Proceedings of the XVIII AIDAA Italian National Congress* [CD-ROM], Assoc. Italiana di Aeronautica e Astronautica, Rome, 19–22 Sept. 2005.

[6] Coiro, D. P., Nicolosi, F., De Marco, A., and Genito, N., "Dynamic Behavior and Performances Determination of DG400 Sailplane through Flight Tests," *Technical Soaring*, Vol. 27, Nos. 1– 2, Jan.– April 2003, pp. 24–32.

[7] de Oliveira, P. H. I. A., Ribeiro, R. P., de Freitas Pinto, R. L. U., Resende, L. S., Coiro, D. P., Nicolosi, F., and Genito, N., "Light Aircraft Instrumentation to Determine Performance, Stability and Control Characteristics in Flight Tests," *SAE Brasil Congress*, Society of Automotive Engineers Paper 2004-01-3474, Warrendale, PA, 2004.

[8] Coiro, D. P., Nicolosi, F., De Marco, A., and Genito, N., "Flying Qualities Analysis of A Three surfaces Aircraft Model," XXIII ICAS Conference, International Council of the Aeronautical Sciences Paper 2002-5.2., Stockholm, Sept. 2002.

[9] Giordano, V., Coiro, D. P., and Nicolosi, F., "Flight Tests, Flight Simulation and V.El. Certification on G97 Light Aircraft," *Proceedings of the XVI AIDAA Italian National Congress* [CD-ROM], Assoc. Italiana di Aeronautica e Astronautica, Rome, 24–28 Sept. 2001.

[10] Perkins, C. D., Dommasch, D. O., and Durbin, E. J., *AGARD Flight Test Manual, Vol. I: Performance*, Pergamon, New York, 1959.

[11] Ward, D. T., and Strganac, T., *Introduction to Flight Test Engineering*, Kendall/Hunt Publ., Dubuque, IA, 2000.

[12] Kimberlin, R. D., *Flight Testing of Fixed Wing Aircraft*, AIAA Education Series, AIAA, Reston, VA, 2003.

[13] Anderson, M. W., "Flight Test Certification of Primary Category Aircraft Using TP101-41E Sportplane Design Standard," *Journal of Aircraft*, Vol. 32, No. 3, 1995, pp. 631–635. doi:10.2514/3.46766

[14] Rogers, D. F., "An Engineering Flight-Test Course Emphasizing Flight Mechanics Concepts," *Journal of Aircraft*, Vol. 39, No. 1, 2002, pp. 79–83. doi:10.2514/2.2898

[15] "Airworthiness Standards: Aircraft Engines," Federal Aviation Admin., FAR 33, Washington, D. C., 10 June 1964.

[16] Coiro, D. P., Marulo, F., Nicolosi, F., and Ricci, F., "Numerical, Wind Tunnel and Flight Tests for P92J and P96 Light Aircraft," *XXI ICAS Conference*, International Council of the Aeronautical Sciences, Paper 98-3.11.2, Stockholm, Sept. 1998.

[17] Iscold, P. H., Alvares, F., Salis, N., and Maciel, B., "Development of Light Aircraft Flight Test Equipment," AIAA Atmospheric Flight Mechanics Conference and Exhibit, AIAA Paper 2006-6004, Aug. 2006.

[18] Bossert, D. E., and Wolf, J. D., "Design And Application of a Flight Test Instrumentation System for Education/Research," AIAA Atmospheric Flight Mechanics Conference and Exhibit, AIAA Paper 2001-4313, Aug. 2001.

[19] Nicolosi, F., De Marco, A., and Della Vecchia, P., "Flight Tests of a Twin-Engine Aircraft: Performances, Stability and Parameter Estimation," *Proceedings of the XX AIDAA Italian National Congress* [CD-ROM], Assoc. Italiana di Aeronautica e Astronautica, Rome, June 2009.

[20] Coiro, D., Nicolosi, F., Scherillo, F., and Maisto, U., "Single Versus Multiple Winglets: Numerical and Experimental Investigation," *Proceedings of XXVI ICAS Congress*, International Council of the Aeronautical Sciences, Paper 2008-2.7.3, Stockholm, Sept. 2008.

[21] "Flight Test Guide for Certification of Part 23 Airplanes," Federal Aviation Admin. Advisory Circular 23-8A, Washington, D. C., Feb. 1989.

[22] Kohlman, D. L., "Flight Test Results for an Advanced Technology Light Airplane," *Journal of Aircraft*, Vol. 16, No. 4, 1979, pp. 250–255. doi:10.2514/3.58513

[23] Taylor, T., Bennett, G., Coble, D., and Hall, K., "A Flight Test Study to Determine Aircraft Propulsive Efficiency and Aerodynamic Drag Using Two Parameter Identification Methods and Lock's Propeller Model," 30th Aerospace Sciences Meeting and Exhibit, AIAA Paper 1992-0170, Jan. 1992.

[24] "Flight Test Guide for Certification of Part 23 Airplanes," Federal Aviation Administration, Advisory Circular 23-8B, Washington, D. C. Feb. 1989.

[25] Srinathkumar, S., Parameswaran, V., and Raol, J. R., "Flight Test Determination of Neutral And Maneuver Points of Aircraft," AIAA Atmospheric Flight Mechanics Conference, AIAA Paper 1995-3501, Aug. 1995.